Nanoscale

Visualization of molecular binding sites at the nanoscale in the lift-up mode by amplitude-modulation atomic force microscopy

Journal:	*Nanoscale*
Manuscript ID	NR-ART-08-2020-006125.R2
Article Type:	Paper
Date Submitted by the Author:	22-Jan-2021
Complete List of Authors:	Maekawa, Tatsuhiro; Tokyo Institute of Technology, Department of Materials Science and Engineering, School of Materials and Chemical Technology Nyu, Takashi; Tokyo Institute of Technology, Department of Materials Science and Engineering, School of Materials and Chemical Technology Mondarte, Evan Angelo; Tokyo Institute of Technology, Department of Materials Science and Engineering, School of Materials and Chemical Technology Tahara, Hiroyuki; Tokyo Institute of Technology, Department of Materials Science and Engineering, School of Materials and Chemical Technology Suthiwanich, Kasinan; Tokyo Institute of Technology, Department of Materials Sciences and Engineering Hayashi, Tomohiro; Tokyo Institute of Technology, Department of Materials Science and Engineering, School of Materials and Chemical Technology

ARTICLE

Visualization of molecular binding sites at the nanoscale in the lift-up mode by amplitude-modulation atomic force microscopy

Received 00th January 20xx,
Accepted 00th January 20xx

DOI: 10.1039/x0xx00000x

Tatsuhiro Maekawa[a,*], Takashi Nyu[a,*], Evan Angelo Quimada Mondarte[a], Hiroyuki Tahara[a], Kasinan Suthiwanich[a], and Tomohiro Hayashi[a,b,#]

We report a new approach to visualize the local distribution of molecular recognition sites with nanoscale resolutions by amplitude-modulation atomic force microscopy. By integrating chemical modification of probes, photothermal excitation to drive cantilever, and lift-up scanning over surface topography, we successfully visualized binding sites provided by streptavidin on a solid surface for biotin attached on AFM probe. The optimization of measurement conditions was discussed in detail, and the application of the technique was verified with a different ligand-receptor system.

Introduction

Visualization of molecular binding sites at nanoscales is one of the most in-demand techniques in biology and biosensing. For the former, especially in cell biology, the local distribution of receptor molecules on a cell membrane and the distribution's temporal evolution provide valuable information on mechanisms underlying the responses of cells to external stimuli such as ions and cytokines.[1, 2] For biosensing applications, the distribution of receptor molecules on sensing surfaces is a critical factor directly governing the sensitivity of the sensors.[3, 4]

We usually labeled ligand molecules to visualize receptor molecules' binding sites for ligands by fluorescence (FL) microscopy. However, to follow the temporal change in the distribution of the binding sites, we need the tedious repetition of injecting the ligands and rinsing at certain time intervals. Genetic modification to express green fluorescent proteins (GFP) is an alternative to the labelling method for real-time monitoring.[5] Since gene recombination is essential for using this method; the measurement process becomes complicated. Therefore, a visualization method without labelling has been in demand. As to biosensors, the receptors' density and their orientation and conformational change of the receptor molecules influence the sensor's performance. The observation by FL microscopy does not provide any information on this.

Force-mapping by atomic force microscopy (AFM) enables us to visualize the surface topography and the receptors' binding capability simultaneously by analyzing the force curves measured at each point.[6-11] In this measurement, ligand molecules are chemically attached to the surface of the probe. The specific interaction between the ligand and receptor appears as adhesion force in a retracting curve. One major drawback of this approach is a long measuring time. Although the imaging time depends on the number of data points (pixels) in an image, it sometimes takes several hours. In such cases, we cannot monitor a temporal change in the distribution of receptors in a membrane of living cells. To overcome this drawback, techniques to measure force curves at a high frequency (50 to 1000 Hz). However, even with these methods, the imaging time still takes at least 10 to 15 minutes.[12]

Amplitude-modulation (AM) AFM is currently the fastest mode among various imaging modes. In particular, high-speed AFM was able to visualize the motion of biomolecules at video rates and became one of the essential tools in the field of biophysics.[13, 14] AM-AFM also provides information on adhesion between probe and sample and the local viscoelastic property from the phase difference between excitation and oscillation of the cantilever. Therefore, AM-AFM has the potential for high-speed visualization of molecular binding sites.

However, several technical issues need to be solved to employ AM-AFM to visualize molecular binding sites. The first issue is the stability of the phase-shift imaging in liquid. In the most conventional acoustic excitation system for driving the cantilever, the resonance curve shows multiple spurious peaks around the main resonant peak because of hydrodynamic modes of the surrounding liquid, resonances of the liquid cell, and the piezoelement.[15, 16] This causes a hopping between spurious resonant modes during measurement affecting the quality of the phase-shift images. Another issue is the influence

[a] Tokyo Institute of Technology, Department of Materials Science and Engineering, School of Materials and Chemical Technology, 4259 Nagatsuta-cho, Midori-ku, Yokohama, Kanagawa 226-8503, JAPAN.
[b] JST-PRESTO, 4-1-8 Hon-cho, Kawaguchi, Saitama 332-0012, JAPAN
#˚Equally contributed to this work as the first author
#Corresponding author: tomo@mac.titech.ac.jp
Electronic Supplementary Information (ESI) available: Imaging results of a BSA-BSA antibody system. See DOI: 10.1039/x0xx00000x

of surface topography, adhesion, and viscoelastic response of the sample to the phase shift signal.[17, 18] A method has to be devised to extract the info only on molecular binding events from the phase shifts.

We integrated several techniques in this work, including photothermal excitation, phase-shift imaging, and chemical modification of probes to realize high-speed visualization of molecular binding sites. We present a comprehensive discussion on optimizing the measurement conditions, the accuracy of the detection, and our technique's versatility.

2. Materials and methods

2.1 Atomic force microscope and cantilevers

We used the commercial AFM instrument (MFP-3D Bio, Oxford Instruments, USA) equipped with a liquid cell and home-made photothermal excitation system. All measurements were performed in PBS at room temperature (300 K).

AFM cantilevers (BioLever mini, Olympus, Japan) with Si_3N_4 tips, a nominal spring constant of 60 pN/nm, and a resonance frequency of 25 kHz in water were chosen. Spring constants of cantilevers were calibrated by measuring the thermal noise.[19] The deflection sensitivity was calculated from the slope of the linear compliance region in the force-distance curve. Besides, the sensitivity for a freely moving cantilever was calculated using a method proposed by Walters et al.[20, 21]

2.2 Home-made photothermal excitation system

For AM-AFM imaging, we employed photothermal excitation to drive the cantilevers.[22, 23] In this system, an intensity-modulated laser light (405 nm in wavelength, NovaPro, RGB Photonics GmbH, Germany) was irradiated on the backside of the cantilever to control its resonant amplitude within 0.5 – 50 nm(Fig. 1). In this work, the resonant amplitude was fixed at 10 nm.

2.3 Force-spectroscopic measurements

In force-distance curve measurements in a contact mode, we set the triggering force on approaching and the loading speed at 170 pN and 500 nm/sec, respectively. To obtain the tip-surface separation distance from the cantilever's deflection, we defined the separation of zero as where linearity in the constant compliance region started in the force-distance curve.[24] All of the curves measured in the contact mode were acquired by raster scanning an area of 20 × 20 μm² with 170 × 170 points (totally 28900 curves). The force curves were processed with our original software under Igor Pro (WaveMetrics, inc) to evaluate adhesion force.

2.4 Lift-up scan for molecular recognition imaging

A lift-up scan (LUS) mode (sometimes denoted as LiftMode and nap mode in commercial systems) was employed to visualize sites for molecular recognition (Fig. 2). In a line scan, surface topography was acquired by usual AM imaging at the set amplitude of 6 nm (amplitude in a free state is 10 nm). Then, the phase shift was monitored along with a trajectory that is higher with Δ*h* than the topography measured in the first scan.

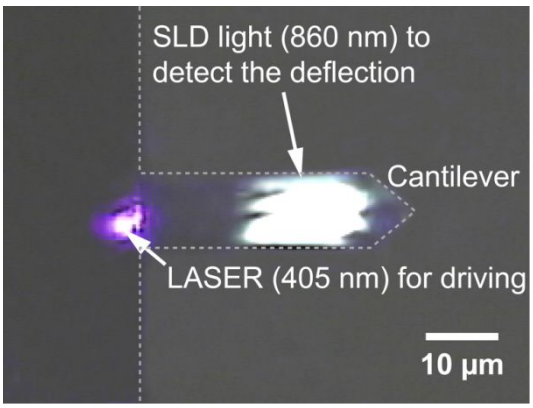

Figure 1. Microscope image of the AFM cantilever irradiated on the back-side by a superluminescent diode (SLD) light for detection and a LASER for photo-thermal excitation.

These two scannings were performed alternately. A scan size was 2 × 2 μm^2 with 512 lines.

2.5 Fabrication of self-assembled monolayer substrates and immobilization of streptavidin on the surface

Si (Furuuchi Chemical, Japan) substrates were cleaned by repeating ultrasonication in deionized water (PURELAB flex-3, ELGA, UK) for 15 min three times and dried with a nitrogen gas stream. After that, the Si substrates were cleaned by a UV/ozone dry stripper (UV-300, SAMCO, Japan) for 15 min. Moreover, Au/Ge/Si substrates were fabricated by thermal evaporation of Au (99.999%, Furuya Metal, Japan) and Ge (adhesion promotor) (The Nilaco Corporation, Japan) under a vacuum pressure of around 2 × 10^{-6} Pa. To control the density of streptavidin molecules on the substrates, self-assembled monolayers (SAMs) were fabricated from two precursor thiol molecules with different terminal groups: $HSC_{11}(EG)_6OCH_2COOH$ and $HSC_{11}(EG)_3OH$ (ProChimia Surfaces, Poland). A thiol solution at a concentration of 1 mM was prepared by dissolving $HSC_{11}(EG)_6OCH_2COOH$: $HSC_{11}(EG)_3OH$ in

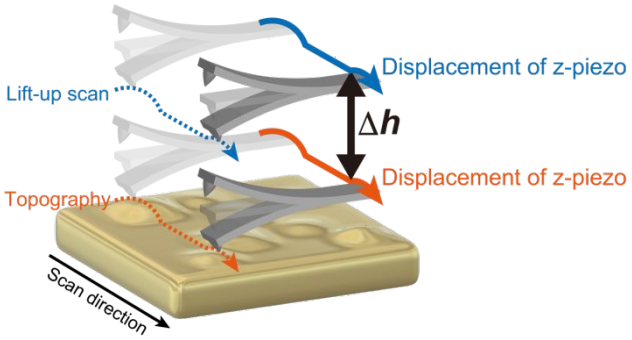

Figure 2. Schematic image of the LUS mode. In the first scan, topographic data was obtained by scanning in the usual AM mode (1st scan). Then, in the second scan, the phase was monitored along the trajectory (could not understand what we mean by "along the trajectory") Δ*h* higher than the topography obtained in the first scan.

ethanol (5 mL, Wako, Japan) at a molar ratio of 1:3. To activate the –COOH terminal groups for forming an amide bond with –NH_2 terminal groups of streptavidin molecules, the SAM substrates were immersed in a solution of N-hydroxysuccinimide (NHS, 75 mM, KANTO CHEMICAL, Japan) and 1-ethyl-3-(3-dimethylaminopropyl)carbodiimide hydrochloride (EDC, 300 mM, Tokyo Chemical Industry, Japan) in deionized water for 30 min. Finally, streptavidin molecules were immobilized to the activated –COOH terminal groups on the substrates by immersing the substrates in a solution of streptavidin (SA) (Sigma-Aldrich, USA) dissolved in phosphate-buffered saline (PBS, Sigma-Aldrich, USA) for 2 h.[25]

2.6 Functionalization of AFM probes with biotin molecules

The AFM probes (BioLever mini, Olympus, Japan) were cleaned beforehand by UV/ozone dry stripper for 15 min, then with 0.1 M hydrochloric acid solution. They were then rinsed with deionized water and dried with a nitrogen gas stream. For the functionalization of the probe tips, a solution of (3-aminopropyl)triethoxysilane (APTES, Tokyo Chemical Industry, Japan) and triethylamine (TEA, Wako, Japan) at a volume ratio of 3:1 was prepared under nitrogen atmosphere. APTES forms a SAM on the tip surface, while TEA catalyzes the reaction. The probes were placed in a sealed box together with the APTES/TEA solution allowing the vapor molecules to attach to the tip surface for 3 *h* in a nitrogen atmosphere, activating the surface with a primary amine terminal group. Next, α-Biotin-(ethylene glycol)$_{24}$-ω-succinimidyl propionate (Biotin-dPEG$_{24}$-NHS, Quanta BioDesign, USA) and α-Methoxy-(ethylene glycol)$_{24}$-ω-propionic acid succinimidyl ester (MeO-dPEG$_{24}$-NHS, Quanta BioDesign, USA) were dissolved in PBS (1 mM) at a volume ratio of 1:5 to control the density of biotin molecules. [26] Finally, the probes were immersed in the mixture solution for 12 *h* to form a crosslink between the NHS end and the amine terminal group.

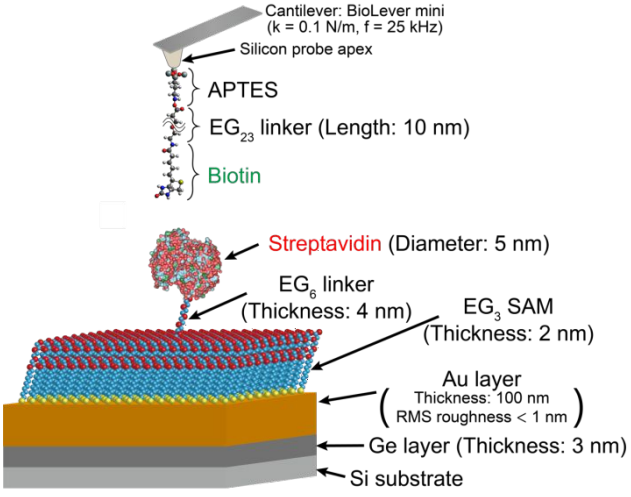

Figure 3. Schematic illustration of the biotin-modified AFM cantilever and the streptavidin-immobilized SAM substrate used in this work.

A schematic image of the overall system using the biotin-modified cantilever and the streptavidin-immobilized substrate is shown in Fig. 3.

3. Results and discussion

3.1 Stability of phase imaging

First, we investigated an amplitude-drive frequency curve with conventional acoustic excitation. In Fig. 4 (a), we see "the forest of peaks" in both amplitude- and phase-driving frequency curves, indicating that a considerable number of spurious resonant modes exist around the true resonant peak. This condition affected the stability in phase-shift imaging, even though a stable topographic image was possible to obtain [Fig. 4 (b) and (c)]. In contrast with the acoustic excitation, our photothermal excitation system generated a smooth resonant curve with only one main peak for [Fig. 4(d)]. Consequently, we avoided the occurrence of the mode hopping in our subsequent results. It should be noted that several works succeed in a stable phase imaging with a bare tip using the acoustic excitation. However, in our measurements discussed below, we could not perform stable phase imaging with the acoustic excitation. We consider that the strong interaction between SA and biotin may promote the mode hopping.

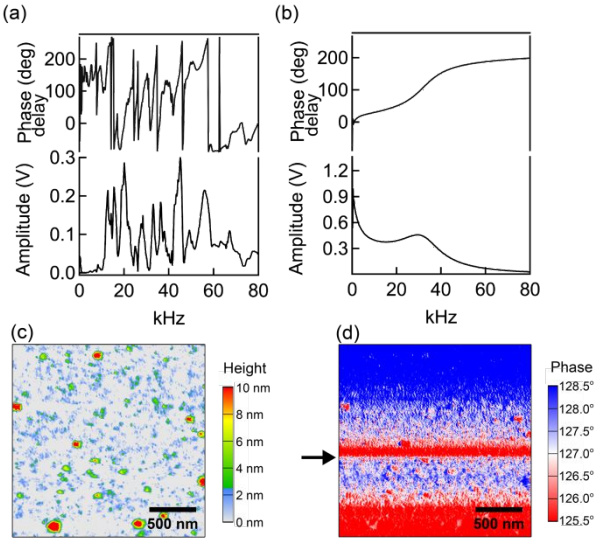

Figure 4. Phase- and amplitude-driving frequency plots showing the cantilever drive response with the (a) acoustic and (b) photothermal excitation. (c) Height and (d) phase shift images of the streptavidin-immobilized SAM substrate obtained with the biotin-modified tip through acoustic excitation. The arrow indicates the scanning line where the mode hopping occurred.

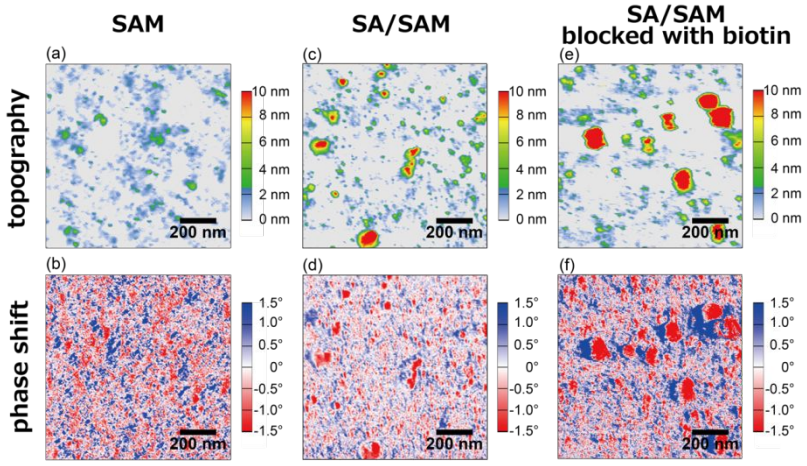

Figure 5. AM-AFM (a) height and (b) phase images of the SAM/gold substrate; (c) height and (d) phase images of the SA/SAM/gold substrate; and (e) height and (f) phase images of the substrate after blocking the binding sites of SA with biotin.

3.2 Imaging of the molecular recognition events by normal scanning in AM mode

Normal AM imaging with feedback maintaining a constant amplitude (free and feedback amplitudes are 10 and 6 nm, respectively) was performed to initially inspect the topographic and phase shift profiles of our SAM substrates with and without the immobilized SA molecules. The topographic image of the pure OEG-SAM exhibited surface morphologies of less than 3 nm [Fig. 5(a)] and showed a weak correlation to its corresponding phase shift image [Fig. 5(b)]. On the other hand, the sample with immobilized SA showed protrusions with a height of 5-10 nm [Fig. 5(c)], in agreement with the diameter of an SA molecule (about 5 nm) immobilized via an OEG linker (1 nm in length).[27-29] These high topographic regions corresponded to the large phase lag regions in the phase shift image [Fig. 5(d)], implying that the molecular recognition events could be detected as phase lags. However, a similar phase lag is also observable in regions with no protrusions. Also, similar to what was observed in the pure OEG-SAM images, the phase shifts in other areas do not correspond to any structures in the surface topography.

Similar results can also be observed on the biotin-blocked sample, which was fabricated by dropping a biotin solution on the SAM substrate with immobilized SA molecules [Fig. 5(e) and (f)]. Positive and negative phase shifts were also detected frequently across the sample and even at the high protrusions that could correspond to the SA molecules with supposedly blocked binding sites. These results show that these phase shifts were also clearly affected by the SAM surface geometry and viscoelasticity other than detecting the molecular recognition events. Therefore, it is difficult to detect only the molecular recognition event by phase imaging in the AM mode if the tip scans the surface in close proximity.

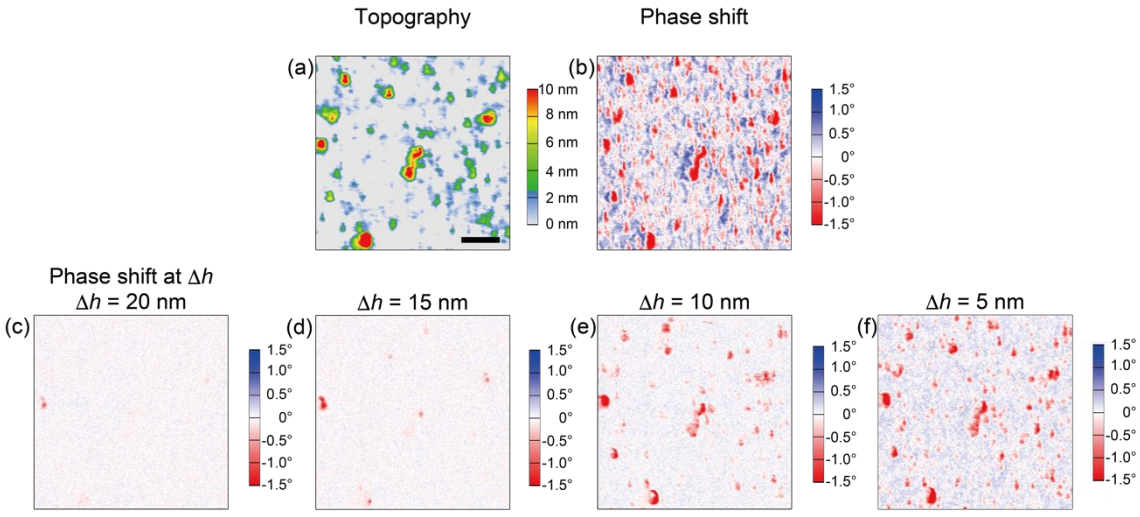

Figure 6. (a) Height and (b) phase shift images at the sample surface (first scan) and phase shift images obtained at Δh = (c) 20, (d) 15, (e) 10, and (f) 5 nm. All images are in the same scale (the black scale bar in (a) corresponds to 200 nm).

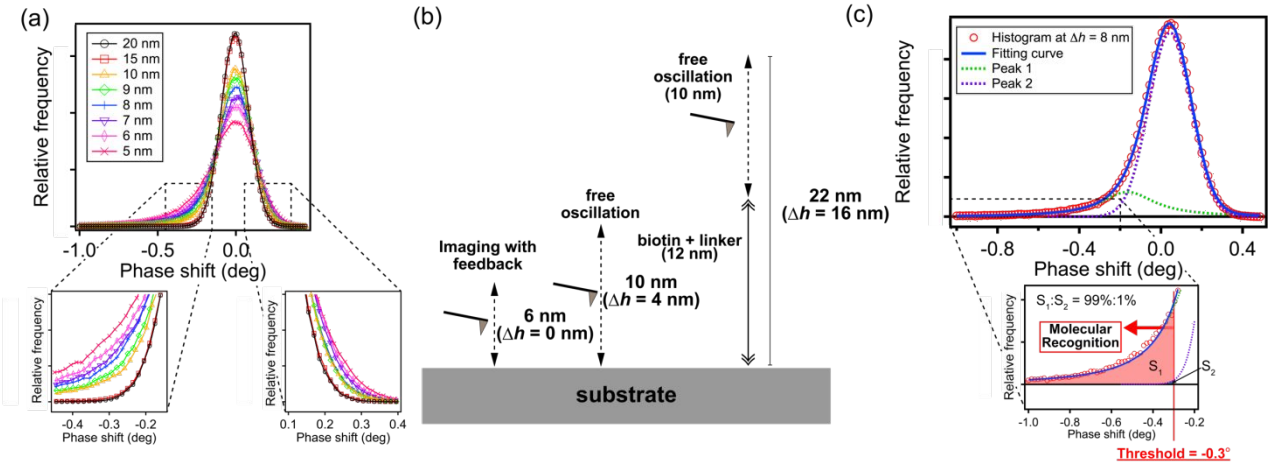

Figure 7. (a) Distributions of the phase shift in LUS images obtained with Δh = 20, 15, 10, 9, 8, 7, 6 and 5 nm in the same area. (b) schematic diagram to explain the relation among amplitude of the cantilever (dotted line), full length of the molecule immobilized on the tip and Δh. (c) The distribution at Δh = 8 nm (red circles) and the fitting curve (blue line). The dotted lines are the result of the peak deconvolution showing the influence of the molecular recognition (Peak 1) and sample surface (Peak 2) on the detected phase shifts.

3.3 Molecular recognition imaging by the LUS mode and evaluation of optimal Δh

Through LUS mode (Fig. 2), we were able to diminish the influence of surface geometry and viscoelasticity on our measurements on the phase shift. We evaluated the optimal Δh in which the molecular recognition events could be dominantly detected.

By performing the scans on the same surface with a topography and phase shift profile shown in Fig. 6 (a) and (b), respectively, the results show that the number of regions with detected phase lags increases as Δh is decreased [Fig. 6(c)-(f)]. In the case of Δh = 20 and 15 nm, even with the oscillation free amplitude of 10 nm, there was difficulty in establishing the specific interaction of streptavidin and biotin. At Δh = 10 nm, which corresponds to the length of the PEG linker, more regions with phase lags appeared in the phase image. Further decreasing the Δh to 5 nm resulted to even more and larger phase-lag regions and more phase shifts across other regions with lower protrusions (≤ 5 nm). In this case, the cantilever probably reached closer to the sample surface affecting the oscillation phase of the cantilever during the scan.

We further scanned the sample at the Δh-range of 5-10 nm at 1 nm increment to quantitatively evaluate the optimal Δh by analyzing the detected phase shifts [Fig. 7(a)]. The distribution for Δh = 20 and 15 nm has shown to be highly symmetrical with respect to phase shift = 0°. By considering the chemical structure of the modified probe (total molecular length of APTES, PEG linker, and biotin are connected via PEG linker with a length of 12 nm) and free and target amplitudes of the cantilever (10 and 6 nm, respectively), it is possible to expect that the biotin moieties can contact the surface with Δh between 0 and 16 nm [Fig. 7(b)]. Note that the PEG moieties do not always take an all-trans configuration. Therefore, the contact between the tip and substrate theoretically occurs at smaller than Δh = 16 nm. A significant flattening and broadening of the distributions can be observed at Δh = 10 nm, implying an increased signal detection.

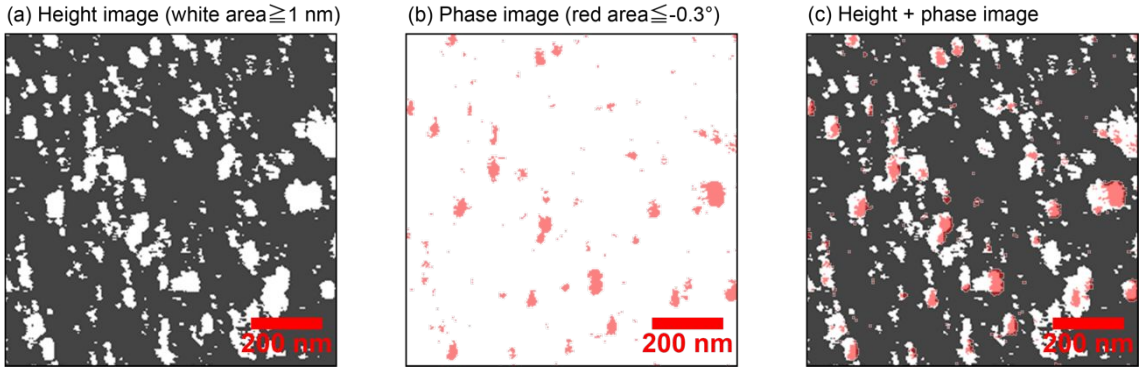

Figure 8. (a) A binarized height image from AM mode (threshold = 1 nm). (b) A binarized phase image from LUS mode at Δh = 8 nm (threshold = -0.3°). (c) Combined image by superimposing (a) and (b).

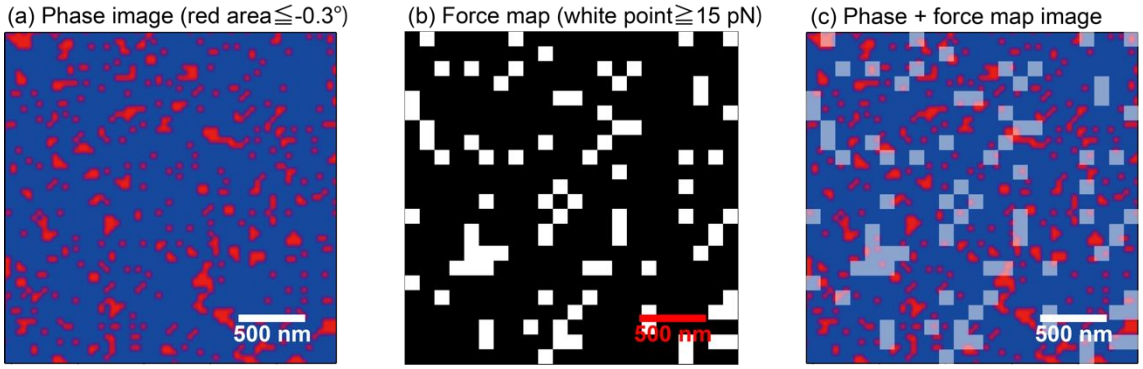

Figure 9. (a) A binarized phase image from LUS mode at Δ*h* = 8 nm (threshold = -0.3°). (b) A binarized force map (threshold = 15 pN). (c) Combined image by superimposing (a) and (b).

Moreover, the distributions display skewness to the negative phase shift region, which would imply that the phase lags caused by the specific interaction of the molecular recognition were detected predominantly while receiving slight influence from the surface. In detail, the results at Δ*h* = 10, 9, and 8 show that while the distributions of regions with the positive phase shifts were overlapping, more of the higher phase lag signals were detected as the scan came closer to the surface. This indicates an increased detection of the molecular recognition events while the influence from the surface hardly changed. Decreasing the Δ*h* to 7, 6, and 5 nm resulted in the further broadening of the positive phase shift region, showing that the oscillation phase of the cantilever was increasingly influenced by the sample surface together with the molecular recognition. For these reasons, we defined 8 nm as the optimal value for Δ*h* in LUS mode, which enabled the detection of the molecular recognition with high sensitivity and minimal influence from the surface.

Through peak deconvolution, we obtained two peaks constituting the distribution at Δ*h* = 8 nm [Fig. 7 (c)]. We attribute Peak 1 to the detected molecular recognition events and Peak 2 to other factors that influence the phase shift, such as the sample surface and the photothermal and detection noise. At phase shift ≦ -0.3°, where the frequency is almost 0 for Δ*h* = 20 and 15 nm, we calculated the peak area ratio for Δ*h* = 8 nm and found to be 99%:1% (Peak 1:Peak 2). This clearly shows that the detected phase lags at ≦ -0.3° are mainly from the molecular recognition events. We then used this threshold to create a binarized phase shift image to determine the correlation of the phase lag regions with the height data obtained by normal AM mode (Fig. 8) and with the conventional force spectroscopic mapping image (Fig. 9).

3.4 Comparison of topography and molecular recognition images

Basing on the root mean square roughness of the Au/Ge/Si substrate, we set a threshold of 1 nm to create a binarized height image [Fig. 8(a)] and superimposed this on the binarized phase shift image [Fig. 8(b)].

Figure 8 (c) clearly shows protrusions, which correspond to the size of SA, with no detected phase lag. It is noteworthy that there is a possibility that some binding sites of SA molecules were oriented in such a way that they were not easily accessible for the ligand molecules. One can consider this occurrence to be analogous to biosensing devices wherein receptor molecules are inactive for detection compromising the biosensor efficiency. Through phase imaging in LUS mode, we could distinguish the active molecular recognition sites from the inactive ones - an advantage over the typical AM-mode imaging.

3.5 Comparison of the results of the molecular recognition imaging and conventional force mapping

We also evaluated the detection sensitivity of the LUS-mode imaging by comparing the result obtained in the force spectroscopic mapping in contact mode. Fig. 9 (c) displays the superimposition of the phase shift image [Fig. 9 (a)] on the force spectroscopic map [Fig. 9 (b)]. We scanned a large area in the two modes, then superimposed them by adjusting the topographic images obtained in the two modes. By analyzing the thermal noise of the force spectroscopic measurements at the baseline, we employed a threshold of 15 pN to create the binarized force spectroscopic map. Mapping points exhibiting an adhesion force of 15 pN or higher were regarded as the molecular recognition sites. The results show that the number of molecule recognition sites observed by the contact mode is less than that detected in the phase image.

With the conditions used in this work, about 85% of the binding sites found by the force-mapping method was also detected by LUS mode. Unfortunately, we cannot quantitatively evaluate both methods' detection sensitivity because of the limited spatial resolution in the force-mapping method in this work. However, we observed that the force-mapping method often passed over the recognition events even in the aggregated SA domain, which provides a higher possibility for molecular binding.

We attribute this higher sensitivity of LUS mode compared with force-mapping mode to the following two reasons. One is that the contact time between biotin and SA. In the force-mapping, the time allowed for forming the SA- biotin bond is about 10 % of the total measurement time. On the other hand, in optimal conditions (Δ*h* = 8 nm in this case), the biotin

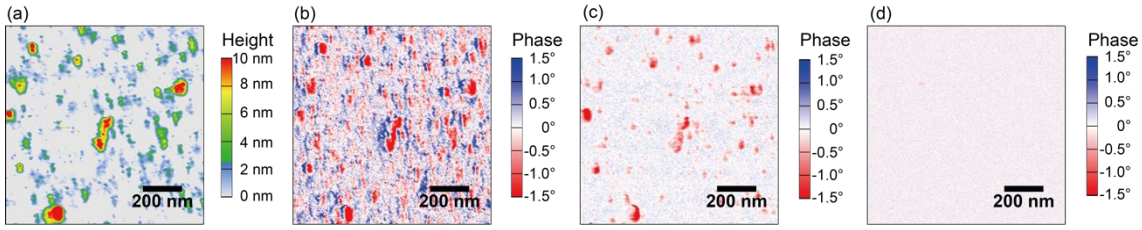

Figure 10. The (a) height and (b) phase shift images by AM mode. The (c) phase shift image by LUS mode at Δ*h* = 8 nm. (d) The phase shift image by LUS mode at Δ*h* = 8 nm after blocking the binding site of SA molecules with biotin. The superimposed image of (a) and (c) is presented in the supporting info.

moieties on the probe continuously have a chance for bond formation.

The second is the difference in the degree of freedom of biotin moiety immobilized to the PEG chain. In the force-mapping, the biotin moiety is confined between the tip and surface under considerable pressure. We previously reported that it is difficult to detect specific interactions unless we held the probe against the sample surface for about 2 sec in the contact mode.[6, 9] Even in the recently-developed fast force mapping or peak force tapping method, we cannot avoid the effect of confinement. In LUS mode, the molecules can maintain a higher degree of freedom because of the weaker confinement originated from the cantilever's oscillation and the lift-up scanning. The conventional or fast force mapping tends to apply substantial force onto biomolecules, resulting in mechanical damage (e.g., conformational change or denaturation) to the biomolecules. By choosing a smaller amplitude, we can further lower the damage to the biomolecules during the scanning.

We compare our method with a similar method called as TREC reported by Hinterdorfer et al.[30] In TREC, the change in the lower half of the oscillation is monitored to acquire the topology of the surface, and that in the upper half is monitored to track molecular binding events. TREC has an advantage over our method in terms of the required number of scanning to obtain an image with the same pixel numbers because TREC can simultaneously evaluate both surface topography and binding sites with keeping a constant height. However, a surface's roughness that can be scanned by TREC is limited by the amplitude. Therefore, our method has an advantage over TREC in scanning a rough surface with a large roughness, such as nano-plasmonic biosensors consisting of nanoparticles or nanodiscs. We are currently evaluating the detection sensitivity of LUS and force-mapping (including conventional force-mapping, peak force tapping, and fast force mapping method) under different conditions to find optimal scanning conditions for each method. The results will be published elsewhere.

3.6 Imaging of a biotin-blocked streptavidin sample in the LUS mode

To confirm that the apparent phase lag regions obtained by the LUS mode at Δ*h* = 8 nm are from the detection of molecular recognition events, we again performed the same measurement after blocking the molecular recognition sites with biotin molecules. Fig. 10 (d) displays that any phase lag was hardly observed in the measurement after the blocking process. This phase image reveals that the biotin molecules effectively blocked molecular recognition sites of streptavidin molecules, indicating that the LUS mode enabled the imaging of the molecular recognition of streptavidin and biotin nanoscale with high sensitivity through the detection of phase delay.

Conclusions

We developed a new technique, which is the combined experimental strategy of photothermal excitation of the cantilever, immobilization of biomolecules on AFM probe, and phase imaging in the lift-up scan mode, to visualize the local distribution of sites for molecular recognition on a solid surface with a nanoscale resolution (~10 nm) at a speed of ~10 min/image. We applied this technique to another ligand-receptor system: bovine serum albumin (BSA) and its antibody (Supporting Information Fig. S3). We also visualized the molecular recognition sites (positions of BSA) clearly using probes functionalized with BSA antibody. The dissociation constant for BSA-BSA antibody (~10^{-8} M)[31] is much higher than that of SA-biotin (~10^{-15} M), indicating that this technique can possibly be applied to other ligand-receptor systems with a weaker interaction than the SA-biotin system.

Among various operation modes of AFM, AM mode is the most promising for fast imaging. In particular, some commercialized AM-AFMs enable us to image samples at video rates (30 frames/sec).[13, 14, 32] We strongly believe that the AM mode, when utilized similarly as our technique – the LUS mode, will contribute to the analysis of a wide range of molecular recognition systems on various surfaces such as the performance evaluation of biosensors and the distribution imaging of membrane proteins on cell membranes with high sensitivity.

Conflicts of interest

There are no conflicts to declare so far.

Acknowledgements

We thank Ms. Kazue Taki for the administration of this work. This work was supported by JST-PRESTO and KAKENHI (JP17K20095 and JP19H02565, and JP20H05210).

Notes and references

1. E. Biener, M. Charlier, V. K. Ramanujan, N. Daniel, A. Eisenberg, C. Bjorbaek, B. Herman, A. Gertler and J. Djiane, *Biol Cell*, 2005, **97**, 905-919.
2. W. D. Heiss and K. Herholz, *J Nucl Med*, 2006, **47**, 302-312.
3. L. M. Bonanno and L. A. Delouise, *Langmuir*, 2007, **23**, 5817-5823.
4. A. Garifullina and A. Q. Shen, *Anal Chem*, 2019, **91**, 15090-15098.
5. M. Chalfie, Y. Tu, G. Euskirchen, W. W. Ward and D. C. Prasher, *Science*, 1994, **263**, 802-805.
6. Y. Arai, K. Okabe, H. Sekiguchi, T. Hayashi and M. Hara, *Langmuir*, 2011, **27**, 2478-2483.
7. P. Hinterdorfer and Y. F. Dufrene, *Nat Methods*, 2006, **3**, 347-355.
8. S. O. Kim, J. A. Jackman, M. Mochizuki, B. K. Yoon, T. Hayashi and N. J. Cho, *Phys Chem Chem Phys*, 2016, **18**, 14454-14459.
9. M. Mochizuki, M. Oguchi, S. O. Kim, J. A. Jackman, T. Ogawa, G. Lkhamsuren, N. J. Cho and T. Hayashi, *Langmuir*, 2015, **31**, 8006-8012.
10. S. L. Xu, M. D. Dong, X. D. Liu, K. A. Howard, J. Kjems and F. Besenbacher, *Biophys J*, 2007, **93**, 952-959.
11. M. Dong and O. Sahin, *Nature Communications*, 2011, **2**, 247.
12. Y. M. Efremov, A. I. Shpichka, S. L. Kotova and P. S. Timashev, *Soft Matter*, 2019, **15**, 5455-5463.
13. G. R. Heath and S. Scheuring, *Nat Commun*, 2018, **9**, 4983.
14. N. Kodera, D. Yamamoto, R. Ishikawa and T. Ando, *Nature*, 2010, **468**, 72-76.
15. C. Carrasco, P. Ares, P. J. de Pablo and J. Gomez-Herrero, *Rev Sci Instrum*, 2008, **79**, 126106.
16. A. O. Volkov, J. S. Burnell-Gray and P. K. Datta, *Applied Physics Letters*, 2004, **85**, 5397-5399.
17. G. Bar, Y. Thomann, R. Brandsch, H. J. Cantow and M. H. Whangbo, *Langmuir*, 1997, **13**, 3807-3812.
18. X. Chen, M. C. Davies, C. J. Roberts, S. J. B. Tendler, P. M. Williams, J. Davies, A. C. Dawkes and J. C. Edwards, *Ultramicroscopy*, 1998, **75**, 171-181.
19. J. L. Hutter and J. Bechhoefer, *Review of Scientific Instruments*, 1993, **64**, 1868-1873.
20. R. Proksch, T. E. Schaffer, J. P. Cleveland, R. C. Callahan and M. B. Viani, *Nanotechnology*, 2004, **15**, 1344-1350.
21. D. A. Walters, J. P. Cleveland, N. H. Thomson, P. K. Hansma, M. A. Wendman, G. Gurley and V. Elings, *Review of Scientific Instruments*, 1996, **67**, 3583-3590.
22. D. Kiracofe, K. Kobayashi, A. Labuda, A. Raman and H. Yamada, *Rev Sci Instrum*, 2011, **82**, 013702.
23. N. Umeda, S. Ishizaki and H. Uwai, *J Vac Sci Technol B*, 1991, **9**, 1318-1322.
24. T. Hayashi, Y. Tanaka, Y. Koide, M. Tanaka and M. Hara, *Phys Chem Chem Phys*, 2012, **14**, 10196-10206.
25. E. A. Mondarte, T. Maekawa, T. Nyu, H. Tahara, G. Lkhamsuren and T. Hayashi, *Rsc Adv*, 2019, **9**, 22705-22712.
26. H. Tahara, T. Nyu, E. A. Q. Mondarte, T. Maekawa and T. Hayashi, *Advances in Materials Physics and Chemistry*, 2018, **08**, 217-226.
27. K. K. Caswell, J. N. Wilson, U. H. Bunz and C. J. Murphy, *J Am Chem Soc*, 2003, **125**, 13914-13915.
28. P. C. Weber, D. H. Ohlendorf, J. J. Wendoloski and F. R. Salemme, *Science*, 1989, **243**, 85-88.
29. H. Yan, S. H. Park, G. Finkelstein, J. H. Reif and T. H. LaBean, *Science*, 2003, **301**, 1882-1884.
30. L. A. Chtcheglova and P. Hinterdorfer, *Seminars in Cell & Developmental Biology*, 2018, **73**, 45-56.
31. W. C. Olson, T. M. Spitznagel and M. L. Yarmush, *Mol Immunol*, 1989, **26**, 129-136.
32. G. E. Fantner, G. Schitter, J. H. Kindt, T. Ivanov, K. Ivanova, R. Patel, N. Holten-Andersen, J. Adams, P. J. Thurner, I. W. Rangelow and P. K. Hansma, *Ultramicroscopy*, 2006, **106**, 881-887.